Journal of Colloid and Interface Science 628 (2022) 437–447

Contents lists available at ScienceDirect

Journal of Colloid and Interface Science

journal homepage: www.elsevier.com/locate/jcis

Ag_5 nanoclusters with dual catalytic antiradical activities

Iria R. Arias [a], David Buceta [a,*], Giampaolo Barone [b], María C. Giménez-López [c], Héctor Lozano [a], Massimo Lazzari [c], M. Arturo López-Quintela [a,*]

[a] Department of Physical Chemistry, Nanomag Laboratory, iMATUS, Universidade de Santiago de Compostela, Spain
[b] Department of Biological, Chemical and Pharmaceutical Sciences and Technologies, University of Palermo, 90128 Palermo, Italy
[c] Center for Research in Biological Chemistry and Molecular Materials (CIQUS), University of Santiago de Compostela, 15782 Santiago de Compostela, Spain

GRAPHICAL ABSTRACT

Ag nanoclusters of 5 atoms, Ag_5, synthesized by a kinetic control method, show exceptional catalytic activities for the redox elimination of radicals. Their use as *catalytic radical scavengers* in industrially relevant processes involving detrimental free radical formation, such as polymer stabilization, is here demonstrated, opening a new class of catalytic antiradicals with many potential industrial and/or biomedical applications.

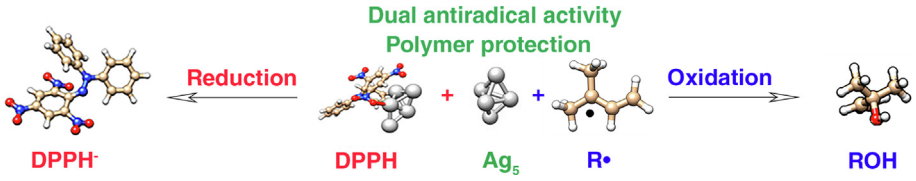

ARTICLE INFO

Article history:
Received 23 May 2022
Revised 20 July 2022
Accepted 21 July 2022
Available online 25 July 2022

Keywords:
Silver nanoclusters
Catalysis
Anti-radicals
Polymer stabilization
Polymer ageing

ABSTRACT

Silver nanoclusters of five atoms (Ag_5) display outstanding catalytic activities for the deactivation of radicals. Using 2,2-diphenyl-1 picrylhydrazyl (DPPH) radical as a model system, we observed a fast radical reduction to DPPH anions using only [Ag_5] 3 to 4 orders of magnitude less than [DPPH]. Moreover, nanoclusters remain stable at the end of the reaction, and can deactivate again DPPH radicals at the same rate, indicating that they act as anti-radical catalysts. The radical scavenger catalytic activity of Ag_5 proceeds selectively through the oxidation of methanol (used to dissolve the radical) to formaldehyde, which is supported by DFT calculations. The obtained catalytic rate constants are almost 2 orders of magnitude higher than oxidases, and more than 4 orders of magnitude larger than graphene quantum dots. We also show that Ag_5 not only catalyze the reduction of radicals but also their oxidation, promoting the inhibition of the autoxidation mechanisms of hydrocarbon polymers, which are very sensitive to the presence of radicals. For this purpose, thin films of two industrially relevant polymers (polyisoprene and acrylonitrile–butadienestyrene copolymer), were exposed to standard simulated photo-ageing conditions in the presence of Ag_5. Using Attenuated Total Reflection-FTIR and DFT modeling we observed that, although Ag_5 nanoclusters, with ≈ 15% surface coverage, do not totally inhibit the oxidation, they favour a decomposition that yields inactive products, in contrast with the more detrimental ketone formation pathway. These results not only open new possibilities for developing a post-process inhibition of polymer degradation, for which nowadays there are no efficient procedures, but also, they could be used as very efficient dual-redox catalytic radical scavengers for different industrial or biomedical purposes.

* Corresponding authors.
E-mail address: malopez.quintela@usc.es (M. Arturo López-Quintela).

https://doi.org/10.1016/j.jcis.2022.07.133
0021-9797/

1. Introduction

Metal nanoclusters, formed by a small number of atoms, show very different properties than both, nanoparticles and bulk, due to the quantum confinement of the free electrons [1]. Such nanoclusters can be seen as super-atoms (or molecules) in which atoms are linked by strong covalent bonds [2]. Among the new properties which emerge at this very small scale (below ≈ 1–2 nm) the catalytic activities show very promising results in different applications [3,4].

Synthetic methods based on kinetic control [5] for the production of nanoclusters of small atomicity in solution can allow the production of nanoclusters with an odd number of atoms (such as Ag_3 or Cu_5 reported before [6,7] or Ag_5, as we recently reported [8]) without a close shell structure, contrary to nanoclusters produced in solution with strong binding ligands or nanoclusters produced in vacuum [9]. Due to the presence of unpaired electrons in such odd number clusters, one should expect a poor stability and a high reactivity of such nanoclusters. Instead of that we observed that they are very stable (see e.g. [2,7,8,10]) in solution without the use of strong binding ligands. Such clusters of very small atomicity without binding ligands show very unusual catalytic properties. For example, Au clusters of ≈ 5 atoms display very high catalytic activities for the aerobic oxidation of thiophenol to disulphide [11]. Very recently, we have also reported exceptional catalytic activities of Ag_5 clusters for the irreversible aerobic oxidation of thiols [8], increasing the catalytic activity in the series $O_2 \ll H_2O_2 <$ OH radicals, which was used to demonstrate a new catalytic approach to cancer therapy [8]. Since Ag_5 clusters promote the catalytic deactivation of OH radicals, we further explored the possibility that such clusters can also act against other type of radicals. We will see here that Ag_5 clusters indeed catalyze the deactivation of other type of radicals, oxidizing or reducing radicals depending on the type of radicals and the species in the media, being susceptible to be reduced or oxidized (respectively).

Free radicals are independently existing chemical substances that can be generated in both chemical and biological systems by multiple pathways, e.g. by the direct cleavage of bonds or electron transfer reactions [12]. To maintain their own stability, radicals formed in living systems attack cells to capture electrons, with resulting functional damage. It is believed that these substances are involved in the cancer growth [13,14] and in some degenerative diseases [15], as well as, cataract, diabetes mellitus, rheumatoid arthritis and cardiovascular diseases [13].

At the same time, radical formation and oxygen addition are the initial steps of a mechanism with enormous practical consequences, as in the well-known autooxidation of hydrocarbons (see Scheme 1) [16].

In the case of feed lipid components this is the major cause of reduction in feed quality, and also the reason of the inexorable deterioration of polymeric materials [17,18]. Thereby, any method or anti-radical substance capable to stop or delay these cycles is expected to have a strong impact on the chain propagation, and the consequent food or polymer stability. As an example, primary anti-oxidants as hindered phenols and secondary aromatic amines are commonly used in polymers to deactivate reactive species formed during propagation or in the secondary cycle, although with many limits concerning their surface migration, decoloring, etc. [19].

In this work, we demonstrate that Ag nanoclusters mainly containing 5 atoms, Ag_5, show, as expected, a high interaction with radicals (as for example the model system 2,2-diphenyl-1-picrylhydrazyl, DPPH). Moreover, and contrary to the expectations, they do not react with the radical, but act as highly selective and efficient catalysts for the *reduction of the radical*. In view of these catalytic anti-radical activities for DPPH, we further explored the possibility to radical elimination in polymers, which indeed it was observed. In this case, Ag nanoclusters catalyze the *oxidation of the radical* producing only *non-radical* species. This completely new outcome has a tremendous potential applicability for use as *catalytic radical scavengers* in industrially relevant processes involving detrimental free radical formation such as polymer stabilization, as we will demonstrate in this work. DFT calculations allowed us to elucidate the involved reaction mechanisms, which unveils their catalytic activities against radicals, opening at the same time a new class of catalytic antiradicals with multiple potential applications.

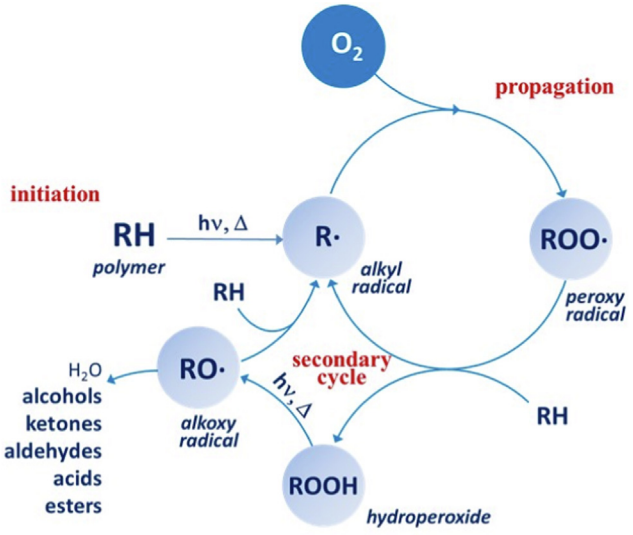

Scheme 1. Simplified mechanism for the autooxidation of hydrocarbons.

2. Materials and methods

2.1. Materials

All the chemicals used in this work (except Ag foils, that were purchased from Goodfellow) were acquired in the commercial brand Sigma Adrich, namely, 2,2-diphenyl-1 picrylhydrazyl (DPPH), methanol HPLC gradient grade, acetone HPLC gradient grade and acetonitrile HPLC gradient grade, sodium chloride (NaCl) 99.99 % and *O*-(2,3,4,5,6-pentafluorobenzyl) hydroxylamine (PFBHA) hydrochloride (>99.0 %).

All aqueous solutions were prepared with MilliQ-grade water using a Direct-Q8UV system from Millipore (Millipore Ibérica S. A., Madrid, Spain). Sandpaper (1,000 grit) was supplied by Wolfcraft España S.L, Madrid, Spain.

2.2. Synthesis of Ag nanoclusters

Silver nanoclusters were electrochemically synthesized using the kinetic control technique [5], by a previously reported method [8].

In short, the synthesis was carried out with a Biologic VMP300 potentiostat (Seyssinet-Pariset, France). A Methrom thermally insulated three-electrode electrochemical cell, deoxygenated just prior to the synthesis, was used with a hydrogen electrode as a reference and two Ag foils (17.5 cm^2 surface area) as counter and working electrodes. Prior to the synthesis, both silver electrodes were polished with sandpaper followed by alumina (≈ 50 nm), washed thoroughly with MilliQ water and sonicated. An ion-

selective electrode was used to verify that, after synthesis, the concentration of remaining Ag^+ ions are always less than 3 mg/L after precipitation with NaCl, and various techniques were used to characterize the synthesized Ag clusters (see below). The samples were finally concentrated at 50 °C using a rotary evaporator (Buchi Rotavapor R-210 at a pressure of 2 mbar) (Massó Analítica S.A., Barcelona, Spain) to a final concentration of ≈ 30 mg/L as determined by flame atomic absorption spectroscopy, performed with a Perkin-Elmer 3110 with a Ag hollow cathode lamp Lumia from Perkin-Elmer (Madrid, Spain) (current 10 mA).

2.3. Characterization methods

UV–vis and fluorescence spectroscopy. Both UV–vis and fluorescence spectroscopy experiments were performed at room temperature using 1 cm path length Hellma quartz cuvettes (Hellma GmbH & Co. KG., Müllheim, Germany). Time-dependent UV–vis spectra were recorded with an Analytik Jena Specord S600 spectrometer (Analytik Jena AG, Jena, Germany) with a diode array detector, and fluorescence spectra were recorded with a Cary Eclipse Varian fluorimeter (Agilent Technologies Spain, S.L., Madrid, Spain).

Atomic force microscopy (AFM). AFM measurements were conducted under normal ambient conditions using an XE-100 instrument (Park Systems, Suwon, South Korea) in non-contact mode. The AFM tips were aluminum-coated silicon ACTA from Park Systems with a resonance frequency of 325 kHz. For AFM imaging, a drop of the Ag_3-AQC diluted sample was deposited onto a freshly cleaved mica sheet (Grade V-1 Muscovite) (Park Systems, Suwon, South Korea), which was thoroughly washed with Milli-Q water and dried under nitrogen flow.

Mass spectrometry. ESI mass spectra were acquired using an LTQ Orbitrap Discovery mass spectrometer (Thermo-Fisher Scientific, Waltham, USA) equipped with an ESI source operating in negative ionization mode. The ESI source conditions were as follows: source voltage −4.5 kV, heated capillary temperature 275 °C, capillary voltage −35 V and sheath gas and auxiliary gas 5 and 2 (N2, arbitrary units). For full-scan MS analysis, the spectra were recorded in the range of *m*/*z* 100 to 2,000 with a scan speed of 1 scan/s. The mass resolution was set at 30,000 FWHM. The Orbitrap instrument was calibrated using a calibration solution according to the manufacturer's instructions. Monitoring experiments were conducted to obtain the maximum sensitivity for the detection of clusters. Solutions were directly injected into the cell after mixing 1 to 1 with an acetonitrile solution with 1 mM NH_4Cl and 0.1 % formic acid.

Ion meter. Ion concentration was measured using a previously calibrated pH & Ion-Meter GLP 22 (Crison Instruments S.A., Barcelona, Spain) by adding a stabilizing solution (sodium nitrate 5 M) at a ratio of 2:100 to the sample at a constant temperature of 25 °C.

Flame atomic absorption spectroscopy. The total Ag content in the cluster samples was analysed by flame atomic absorption spectroscopy, performed with a Perkin-Elmer 3110 with a Ag hollow cathode lamp Lumia from Perkin-Elmer (Madrid, Spain) (current 10 mA).

2.4. DPPH radical deactivation by Ag_5 nanoclusters

The DPPH radical scavenging activity of nanoclusters was evaluated by UV–visible spectroscopy.

A solution of 1×10^{-3} M of DPPH (2,2-diphenyl-1-picrylhydrazyl) was prepared in methanol (acetone or acetonitrile for studying its influence in the kinetic constant). In the experiments, a dilution of that solution was used with a concentration in DPPH of 1.125×10^{-4} M and a quantity of nanoclusters in the range of 20–200 μg/L. Having a ratio 1:3 water: methanol.

After mixture the two compounds (DPPH + Ag_5 nanoclusters), the absorption spectrum was recorded in the range of 250–800 nm and the band of the anionic form (430 nm) was obtained immediately. Then, we recorded spectrums each two minutes, watching that the final of the reaction was achieved in 12–75 min depending on the Ag_5 concentration.

All the experiments were repeated, at least, three times and different blanks were prepared to check the influence of other substances present in the samples of nanoclusters, for instance, NaCl 0.1 M and $AgNO_3$ 35–350 μg/L.

2.5. Analysis of carbonyl compounds by gas chromatography mass spectrometry (GC/MS)

Detection of formaldehyde and any other carbonyl compound formed in methanol DPPH solution was carried by their derivatization to corresponding *O*-(2,3,4,5,6-pentafluorobenzyl)oxime, followed by gas chromatographic separation coupled to mass spectrometer (GC/MS) [20]. The derivatization reagent was prepared by dissolving 50 mg of PFBHA hydrochloride in 10 mL water. Using a microliter syringe, 10 μL PFBHA solution were added to 50 mL of a methanol solution containing DPPH 0.1 mM and, in case, around 10^{-7} M Ag_5 nanoclusters. 5 μL of the resulting solution were injected into the interface (model 1500) of a CDS Pyroprobe 5000, that was coupled through a needle adapter to an Agilent 5975 GC/MS system. The interface was equipped with a quartz liner to limit dead volume and be able to eliminate the salt deposits that form during the analysis. Initially the interface was held (isothermal) at 325 °C, but this appeared to cause instability of the PFBHA producing large peaks of the dimerization product (*m*/*z* 181, M^+ 362). This problem was solved by lowering the interface temperature to 250 °C. For clarity, no pyrolysis reaction was performed; the heated interface is used to separate the salts from the analytes, improving signal quality and protecting the GC/MS instrument. It is worth noting that under these conditions the blank samples do not change colour upon mixing with the PFBHA solution (they remain blue/purple) whereas the samples turn yellow/orange upon contact with the reagent.

A calibration curve was obtained using acetone as internal standard (Fig. S1a). Both the formaldehyde-PFBHA-oxime (M^+ 225) and the acetone-PFHBA-oxime (M^+ 253) have *m*/*z* 181 from the pentafluorobenzyl ion as the base peak at the conditions applied (Fig. S1b). The calculations were performed using the peak area of the base peak. Unreacted PFBHA hydrochloride is detected as *O*-(2,3,4,5,6-pentafluorobenzyl)-hydroxylamine (base peak *m*/*z* 181, M^+ 213) and elutes between the formaldehyde and acetone PFBHA derivatives, as visible in the example in Fig. S1b.

The GC was equipped with a (5 %-phenyl)-methylpolysiloxane HP-5MS column. The method was developed using a fast temperature program and the final data used were performed following the same protocol. The GC was held isothermal (1.5 min) at 60 °C and heated at 20 °C/min to 250 °C. The GC inlet and GC–MS interface were held at 250 °C. The MS operated in EI mode (70 EV). The ion source was held at 230 °C and the single quadrupole MS at 150 °C, scanning in the *m*/*z* range 50–500.

2.6. Accelerated polymer photo-aging

Reference PI is a vulcanized natural *cis*-1,4 polyisoprene for healthcare applications (Semperguard, Semperit Group), with a thickness of 40 μm. ABS copolymer films with a thickness of 100 μm were obtained by extrusion from Magnum 3404 ABS (Dow Chemicals) pellets. In order to investigate the oxidation processes of polymers in times shorter than those necessary under natural conditions, accelerated conditions must be applied. We chose an easily applicable tests of accelerated ageing among those

usually performed to assess polymer durability. Accelerated photodegradation was carried out in a high-speed exposure unit Suntest CPS+(Heraus), equipped with a xenon light source having a constant irradiation at a power of 765 W m^{-2}; a glass filter with cut-off at λ less than 295 nm was used to exclude radiation more energetic than that of outdoor daylight exposure. The maximum temperature of the samples during irradiation was 45 °C black panel temperature. IR absorption spectra in attenuated total reflectance (ATR) mode were collected with a Thermo Nicolet 6700 FTIR instrument equipped with a Smart Endurance device, and a mercury cadmium telluride (MCT) detector, at 4 cm^{-1} resolution for 128 scans. Carbonyl and hydroxyl indexes were normalized against the absorption at around 1445 cm^{-1} ascribed to C—H deformation vibration and considered as approximatively constant during the early stages of oxidation.

2.7. Computational details

DFT calculations were performed to model the energies involved in the redox reaction between Ag_5, hydroxyl anion and DPPH radicals as well as in the methanol to formaldehyde reaction mediated by Ag_5. The M062X [21,22] hybrid functional and the split valence Def2SVP [23] basis set were selected to take account of dispersion and long-range interactions. All calculations were performed with the Gaussian 09 rev E01 [24] software. The geometry of the considered systems was fully optimized in the presence of implicit methanol solvent, by using the "conductor-like polarized continuum model" model [25]. Vibration frequency calculations, within the harmonic approximation, have been performed to confirm that the optimized geometry represented a minimum in the potential energy surface. Low spin (singlet, doublet) and high spin states (triplet, quartet) were analyzed via Hirshfeld method [26] for the DPPH redox reaction as well as in formaldehyde formation.

3. Results and discussion

Clusters were fully characterized by high-angle dark-field scanning transmission electron microscopy (HAADF-STEM), X-ray absorption near edge structure (XANES), electrospray ionisation time-of-flight (ESI- TOF) mass spectrometry, UV–vis, and fluorescence spectroscopy, as it was reported elsewhere [8]. We show in Fig. 1 the UV vis and fluorescence spectra of the used sample. The existence of a main emission band at 388 nm (3.2 eV) can be associated with a quantum size confinement causing a splitting of the Fermi energy levels, and the appearance of a gap between the frontier orbitals HOMO-LUMO (Eg), which increases as the Ag cluster's size decrease. The energy gap, E_g (which can be estimated by the emission peak) is related with the number of atoms in the cluster (N) by the Jellium model ($N = (EF/E_g)$ [3], where EF is the Femi level of the bulk metal (≈5.3 eV for Ag) [6,8]. Using this approach one can estimate that Ag clusters mainly contain 5 atoms. It is to be noticed that a small percentage (≈20 %) of non-catalytic larger clusters (N ≈ 7–9) is also present in the cluster samples, as can be seen by the shoulder in the emission peak at larger wavelengths [6].

3.1. DPPH radical deactivation by Ag_5

Fig. 2 shows the transformation of the radical DPPH into $DPPH^-$ anion and DPPH-H (top) and the corresponding UV–vis spectra (bottom). When aqueous solutions containing Ag_5 were added to a DPPH radical solution in methanol, a fast deactivation of DPPH radicals was spectrophotometrically observed. Fig. 3 shows the time evolution of DPPH in the presence of Ag_5. A progressive and fast decrease of the initial absorption at around 520 nm -corresponding to the radical form (see Fig. 2)- and the corresponding increase of the maximum at 435 nm -corresponding to the anionic DPPH form (see Fig. 2)- indicate an effective transformation of the radical form into the DPPH anion. This means that the DPPH radical deactivation occurs through the reduction of the radical. Moreover, the fact that the reduction of the radical occurs for [DPPH]/[Ag_5] ratios in the range 10^3 –10^4 (see Fig. 4) indicates that nanoclusters are not reacting with the DPPH radical, but they are acting as catalysts. This result is confirmed by the fact that nanoclusters remain unaltered in the solution after the reaction, being able to reduce again the DPPH radical after addition of more amounts of this compound to the reacted solution. This process can be repeated several times without losing the catalytic activity (see Fig. S2). These results confirm both, the stability, and the catalytic action of Ag_5.

The main question to be addressed is which are the species suffering oxidation during the reduction of the DPPH radical. Because of the use of methanol as solvent (due to poor solubility of the radical in water), we hypothesized that this compound could be oxidized, eventually producing formaldehyde, formic acid or other by-products [27,28]. We checked this hypothesis carrying out a series of experiments and analyzing the oxidation by GC/MS. DPPH radical methanol solutions did not show the presence of any oxidation products whereas those DPPH radical solutions containing Ag_5 unveil the formation of only formaldehyde (see Fig. S1b), with a concentration like the DPPH radical used in the experiments, 0.1 mM, indicating the high catalytic selectivity for the alcohol oxidation.

To further corroborate the hypothesis that the methanol is oxidized during the DPPH radical reduction, we carry out the reaction with higher oxidation potential organic solvents, namely, acetone and acetonitrile (see Fig. S3). It is observed that the fastest reaction occurs with methanol, while the kinetic constant is reduced a half

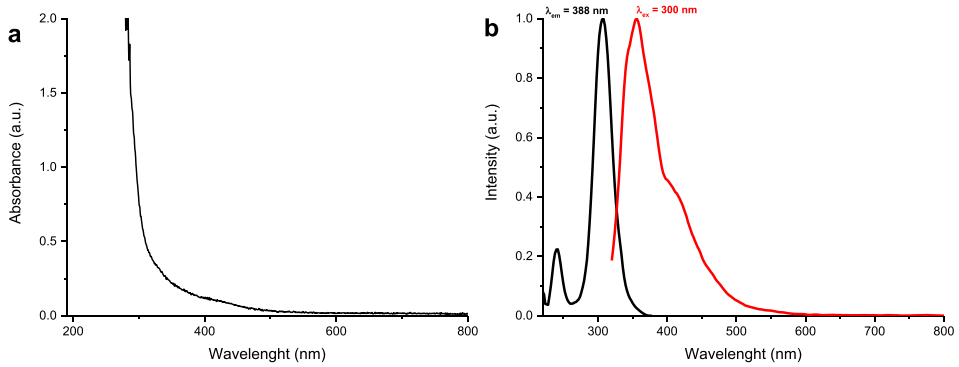

Fig. 1. Absorption (a), excitation at λem = 388 nm (b, black) and emission at λex = 300 nm (b, red) spectra of Ag_5 nanoclusters in water.

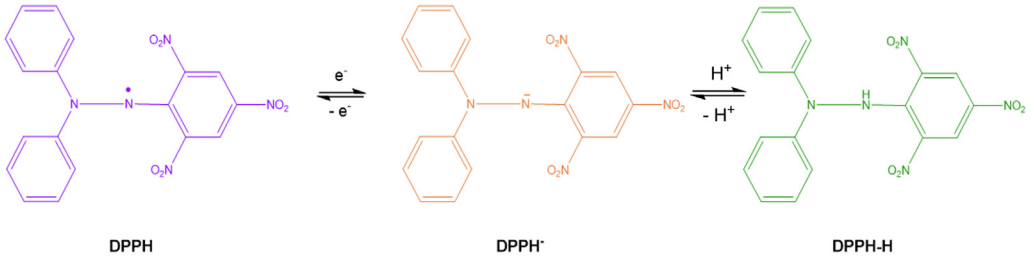

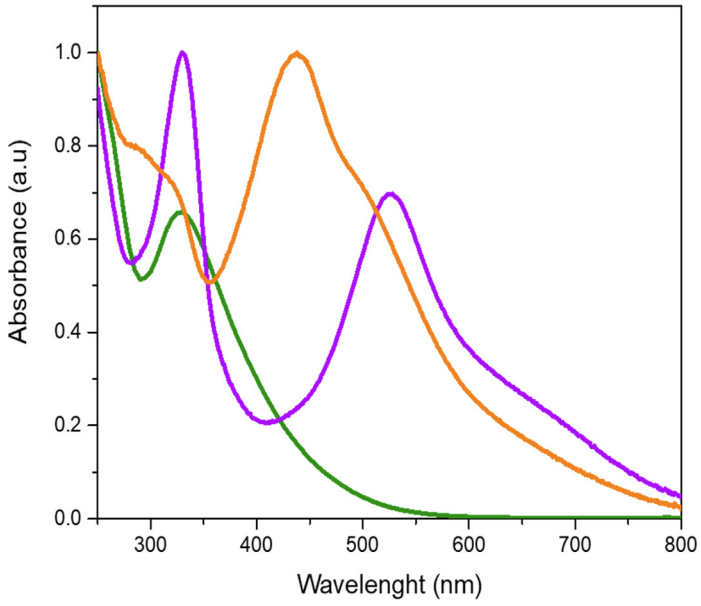

Fig. 2. UV–vis absorption spectra of the radical DPPH, the DPPH⁻ anion, and the protonated DPPH-H compound.

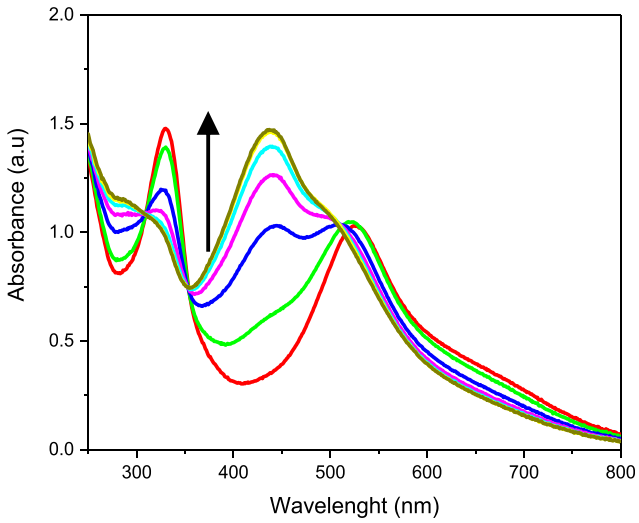

Fig. 3. Time evolution of DPPH (1.125×10^{-4} M) spectra after adding Ag_5 ($\approx 3.7 \times 10^{-7}$M). Spectra were taken every 2 min.

when the reaction media is acetone, and more than 3 orders of magnitude when the reaction is carried out in acetonitrile.

3.2. Kinetic study of DPPH radical deactivation by Ag_5

Fig. 4a shows that the formation of the DPPH⁻ anion is exponential indicating that, in the experimental conditions, the reaction follows a first order kinetics:

$$\frac{d[DPPH^-]}{dt} = k_{obs}[DPPH^-] \quad (1)$$

$$[DPPH^-] = cte - cte' e^{-k_{obs}t} \quad (2)$$

It was further observed that k_{obs} is proportional to the concentration of the catalytic Ag_5 nanoclusters (Fig. 4b):

$$k_{obs} = k_{exp}[Ag_5] \quad (3)$$

From Fig. 4b one can then deduce that $k_{exp} = (1.0 \pm 0.02) \times 10^5$ $M^{-1}s^{-1}$.

To investigate the underlined mechanism of the methanol oxidation by DPPH radical catalyzed by silver nanoclusters, we carried out DFT calculations.

3.3. Charge and spin density analysis of free DPPH (radical and anion form)

We firstly analyze the structure and spin density distribution on both DPPH and Ag_5/DPPH systems. Fig. S4 shows the optimized structure and excess spin density of both DPPH radical (DPPH·, doublet) and DPPH anion (DPPH⁻, singlet). The electron density is homogenously distributed along the entire radical. Table S1 shows the charge and excess spin density distribution by residue. DPPH· charge is distributed as follows: positive charges are located on the diphenylamine residue whereas negative charge lies on the N and trinitrophenyl moieties. Excess spin density is also distributed along the entire radical. The electron transfer from an electron donor to DPPH· yields DPPH⁻ (singlet). This process leads to a redistribution of the charge, and no excess spin density is observed in any of the residues.

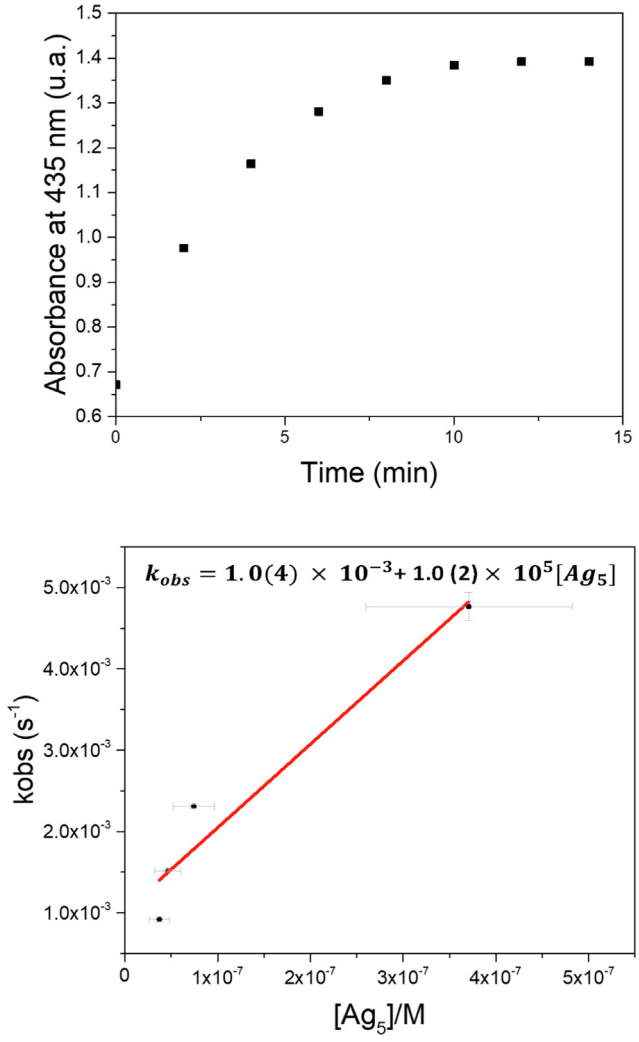

Fig. 4. a) Evolution of the maximum at 435 nm, ascribed to DPPH· 1.12×10^{-4} M in the presence of ≈ 3.7×10^{-7}M Ag_5 in 3:1 (v/v) methanol:water solution. b) Kinetic constant versus [Ag_5] in the range 20–200 μg/L (~3.7×10^{-8}M – ~3.7×10^{-7}M) with a constant DPPH· concentration of 1.12×10^{-4} M in methanol.

3.4. DFT calculations of Ag_5 and DPPH radical in methanol solution

We firstly calculate the formation enthalpy of the different complexes that Ag_5 nanoclusters could form. In order to consider all the species in solution we set the Ag_5 clusters with a continuum/discrete environment. Thus, the main solvent molecules (methanol) were accounted via a polarizable continuum model whereas the species interacting with Ag_5 (methanol, methoxide and DPPH molecules) were accounted by inserting their discrete relaxed structure. We have computed the binding energies of the following systems: Ag_5/methoxide = −164.9 kJ/mol, Ag_5/methanol = −57.7 kJ/mol and Ag_5/DPPH· = −299.3 kJ/mol. From these values it can be assumed that most of Ag_5 are complexed in the form Ag_5/ DPPH·. Although the interaction of this complex with the oxidable species (methanol) could proceed through the methoxide ion or the methanol (p*K*a = 15.5), the most favourable interaction with the methoxide and the need to eliminate a proton during the whole reaction indicates that it is the adsorption of the anion on the Ag_5/DPPH· complex the most preferably pathway to proceed, despite its low concentration in the reaction media (≈ nM).

Fig. 5 shows the DFT-optimized structures and energy of the different steps of the reaction until the formaldehyde and DPPH anion are formed (Table S2 shows the charge and spin analysis for the different intermediate moieties in the reaction). Reaction (1) consists of the adsorption of OCH_3^- anion on Ag_5/DPPH· through the formation of two Ag-O bonds between Ag_5 and one of the nitro groups of DPPH· yielding the Ag_5/DPPH$^-$/OCH_3 system. An electron transfer occurs from the methoxide anion to DPPH radical leading to the formation of methoxide radical and DPPH anion. The adsorption of methoxide anion promotes the presence of excess spin density on the system, thus showing that methoxide anion loses an electron yielding methoxide radical. Charge analysis also reveal that DPPH acquires partial negative charge. This reaction is favored by more than −300 kJ/mol, confirming the experimental finding of DPPH anion formation in the presence of Ag_5 nanoclusters. The next reaction (2) consists of the desorption of DPPH anion from the system. This process leads to the formation of Ag_5/OCH_3 radical with no excess spin density. During this process, the energy increases by + 100 kJ/mol but the subsequent reactions compensate this unfavorable energy. Then, another methoxide anion and another DPPH radical can take part (3). As observed in (1), there is an electron transfer from the methoxide anion to the radical, leading to the formation of Ag_5/DPPH$^-$/$(OCH_3)_2$ with −300 kJ/mol stabilization energy.

Then, the final reaction (**4**) consists in the formation of formaldehyde by a simple hydrogen transfer from one methoxide radical to another, yielding formaldehyde and methanol, with −50 kJ/mol stabilization energy. This reaction occurs in a high spin state. Thus, the Ag_5/DPPH$^-$/CH_2O/CH_3OH system is a quartet in which spin density is located on DPPH anion and in formaldehyde and methanol. Then the system undergoes electronic rearrangements and the spin changes to doublet (**5**). This state is 30 kJ/mol more stable than the quartet state due to the spin stabilization of formaldehyde and methanol that lose its spin density. Finally, the last step consists of the desorption of the attached moieties. The energy balance for this process is almost negligible but due to the affinity of Ag_5 for methanol (−57.7 kJ/mol), the reaction is driven to the formation of Ag_5/CH_3OH, which can be further transformed into the original catalyst (Ag_5/DPPH·) when more DPPH radical is present in the system due to the higher affinity of nanoclusters for the radical (−300 kJ/mol).

3.5. Mechanism

According to the DFT calculations we can propose the following mechanism to explain the kinetic results.

$$Ag_5 + DPPH\cdot + CH_3O^- \rightarrow Ag_5/OCH_3\cdot/DPPH^- \ (1)k_1$$

$$Ag_5/OCH_3\cdot/DPPH^- + CH_3O^- + DPPH\cdot \rightarrow Ag_5 + 2DPPH^- + CH_2O + CH_3OH \ (2)k_2$$

Assuming the steady state approximation for the complex Ag_5/OCH_3/DPPH$^-$, and that the concentration of such complex is much smaller than the concentration of DPPH· and DPPH$^-$, we can arrive at the following expression (see SI for details):

$$\frac{d[DPPH^-]}{dt} = a - b[DPPH^-], \ \text{being.}$$

$a = k_1[Ag_5AQCs]\,[CH_3O^-]\,[DPPH]_0$ and $b = k_1[Ag_5AQCs]\,[CH_3O^-]$

We can observe that this equation agrees with the observed exponential increase of the [DPPH$^-$] and the linear dependence of the kinetic constant with the concentration of nanoclusters. By comparison with the experimental results one can deduce that $k_{exp} = k_1[CH_3O^-] = 10^5\ M^{-1}s^{-1}$. Considering that in the experimental conditions [CH_3O^-] 5 = 3.7×10^{-9}M, we obtain $k_1 = 2.7 \times 10^{13}\ M^{-2}s^{-1}$.

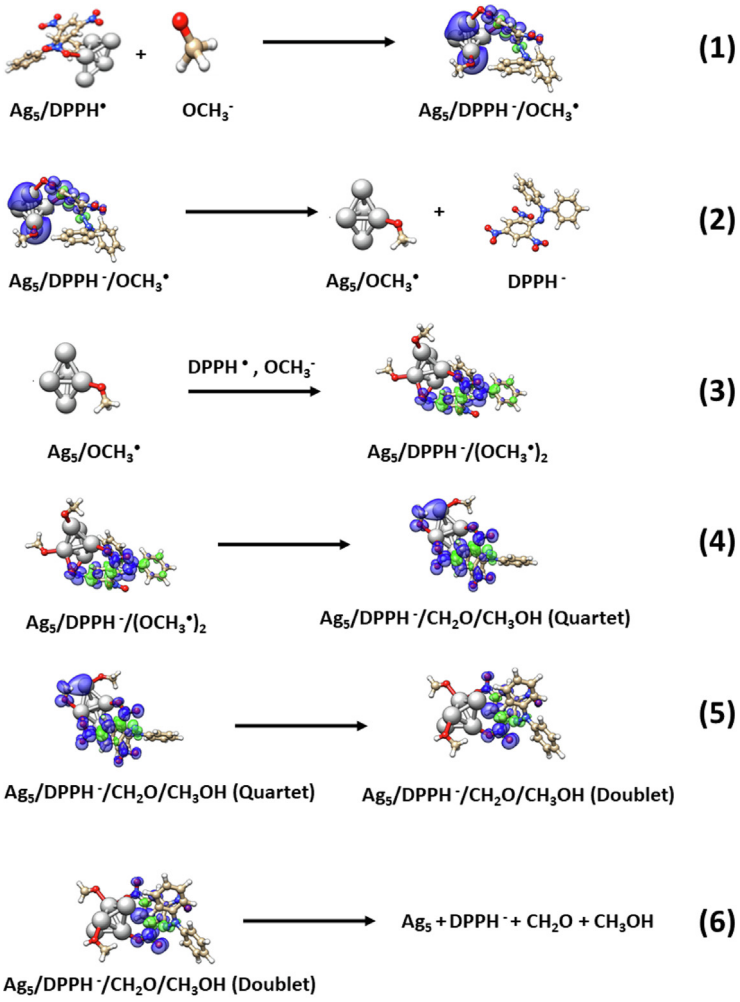

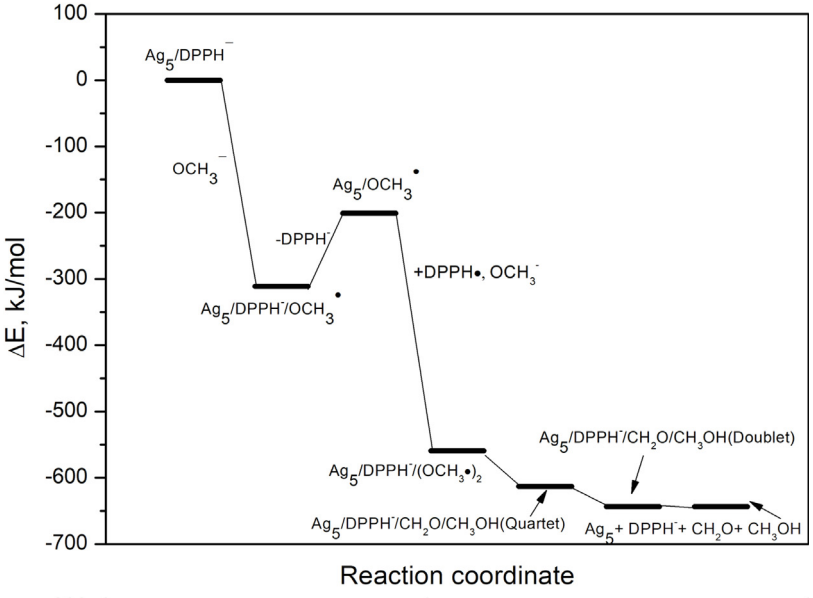

Fig. 5. DFT-optimized structures and energy balance for the oxidation of methanol to formaldehyde by DPPH radical mediated by Ag_5 nanoclusters.

The comparison of the catalytic activity of Ag_5 ($k_{exp} = k_{cat} \approx 1–5 \times 10^{-3}\ s^{-1}$) with some enzymes (oxidases), which are able to catalyze the oxidation of alcohols ($V_{max}/K_M = k_{cat} \approx 1.7 \times 10^{-5}\ s^{-1}$) [29,30] indicates that Ag_5 is almost 2 orders of magnitude more active than oxidases, and with high selectivity to the formation of aldehydes. At the same time, a comparison with graphene quan-

tum dots [31], indicates that DPPH deactivation can be achieved in minutes using a concentration of nanoclusters less than 4 orders of magnitude than quantum dots.

As a conclusion, we can say that the catalytic activation of methanol (a very inactive radical scavenger, which is unable to reduce DPPH radicals) by Ag_5 nanoclusters is highly efficient yielding to a very active radical scavenger with antioxidant properties like other well-known antioxidants, such as polyphenols or vitamin E (see Table S4).This outcome could have important applications in biomedicine, such for the treatment of neurological diseases (Parkinson, Alzheimer, etc.) where free radicals are supposed to be one of the main causes [32].

3.6. Ag_5 as possible protecting agent in polymers

Due to the observed catalytic deactivation of the radical DPPH· by Ag_5 nanoclusters we further explored their application in the possible deactivation of other radicals of industrial interest. For this purpose, we investigated the influence of Ag_5 in the free radical autoxidation mechanism of hydrocarbon polymers. Thin films of two industrially relevant polymers, i.e., polyisoprene (PI) and acrylonitrile–butadienestyrene copolymer (ABS), were exposed to standard simulated photo-ageing conditions. Especially PI provides an excellent model system because of its chemical simplicity and amorphous morphology. Samples were irradiated with a xenon lamp filtered at 295 nm (T < 45 °C), while the structural changes of pristine substrates were compared with those of surfaces bearing around 0.05 μg Ag_5 nanoclusters per cm^2, which implies ≈ 15 % of coverage (see SI for details of this estimation). As expected, pristine polymers undergo the typical radical-based mechanism of autooxidation described in Scheme 1, essentially resulting in the extensive formation of oxygen containing groups [16,33] and low molecular weight products [34]. Using Attenuated Total Reflection (ATR)-FTIR spectroscopy (a direct surface analysis technique) we could observe the formation of hydroxyl groups with a broad band at around 3400 cm^{-1}, and carbonyl groups with a peak at 1720 cm^{-1}, even after just few hours of ageing (see Fig. 6a) [35]. On the other side, development of carbonyl-containing products is more limited in PI treated with nanoclusters, although associated with an extensive hydroxyl formation. Similar behaviour

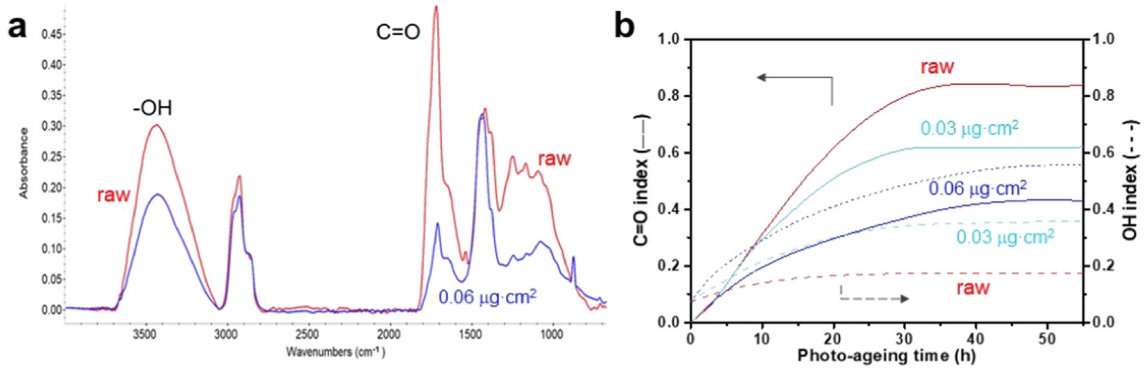

Fig. 6. ATR-FTIR spectra of pristine (red curve) and 0.06 μg cm^{-2} Ag_5-treated PI (blue curve) after 50 h of accelerated photo-ageing (a), and carbonyl and hydroxyl indexes (b), for the pristine polymer (red curves) and 0.03 and 0.06 μg cm^{-2} treated PIs (light blue and blue curves, respectively). Functional group labels indicate main peaks that appear as an effect of ageing.

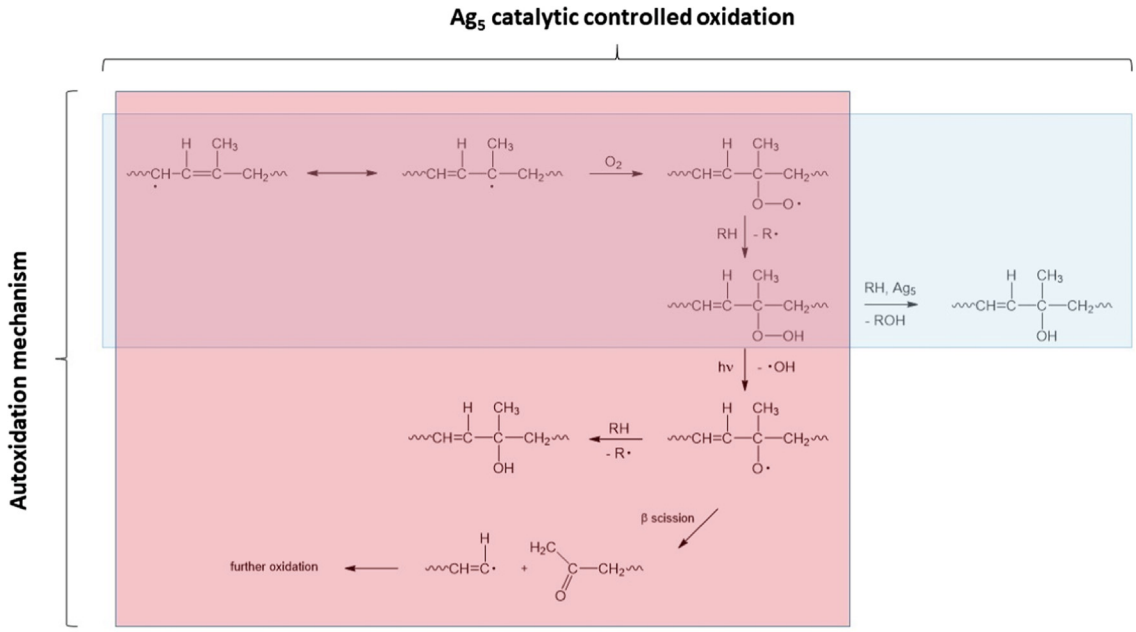

Scheme 2. Most probable pathways of oxidation of raw PI and Ag_5 nanoclusters-treated PI.

was observed for ABS (Fig. S5). ABS is a polymer rather stable against oxidation and the formation of carbonyl and hydroxyl groups as an effect of ageing take place for time longer than in PI, reaching a plateau after around 150 h. As in the case of PI, the oxidation is strongly affected and limited all over the treatment time by the presence of Ag_5 nanoclusters.

The absorbance ratio of either the carbonyl or the hydroxyl band normalized to the intensity of an invariant band offers a convenient comparison for quantifying the relative extent and rate of oxidation (Fig. 6b). Raw and treated PIs achieve a constant level of oxidation after around 30–40 h of ageing, indicating the occurrence of similar oxygen diffusion-controlled processes. However, they reach different values of carbonyl and hydroxyl indexes, which show inverse and directly proportional relationships, respectively, with Ag_5 surface amount. Following the mechanism detailed in Scheme 2 for PI, it is assumed that after the initial unsaturated radical formation, resonance stabilized secondary and especially tertiary alkyl peroxyl radicals are formed by oxygen addition. Subsequent abstraction of hydrogen from the same or another polymer molecule closes the propagation cycle and leads to the formation of hydroperoxides, which easily decompose to tertiary alkoxy and hydroxyl radicals. Further reactions of alkoxy radicals represent the secondary cycle, and mostly results in the formation of either methyl ketones by β-scission or hydroxyl groups via hydrogen abstraction.

Since seminal studies on the effect of structure on the behaviour of alkoxy radicals [36], the relative rates of hydrogen abstraction and β-scission were related to radical stability. In good approximation, the rate of alcohol formation is limited by C—H cleavage and almost independent on the alkoxy radical stability [37], whereas for β-scission the rate and the decrease of activation energy are directly dependent on it. Although at first the presence of Ag_5 seemed to modify such relative rates, DFT modelling for PI oxidation revealed a more favourable route for the hydroperoxide decomposition. Instead of adding a whole PI structure, calculations were performed with 3-methyl-1 butene radical (R·) to mimic the "core" in which autoxidation of PI can occur. Previous computational calculations for nanoclusters in water solutions [8] indicated that Ag_5 could adsorb and activate the adsorbed oxygen molecules. It was observed that $Ag_5/4O_2$ is the most stable structure at P = 1 atm, from T = 298.15 to 500 K (similar results were obtained for Cu_5 nanoclusters [10]). In this conformation, the state of the

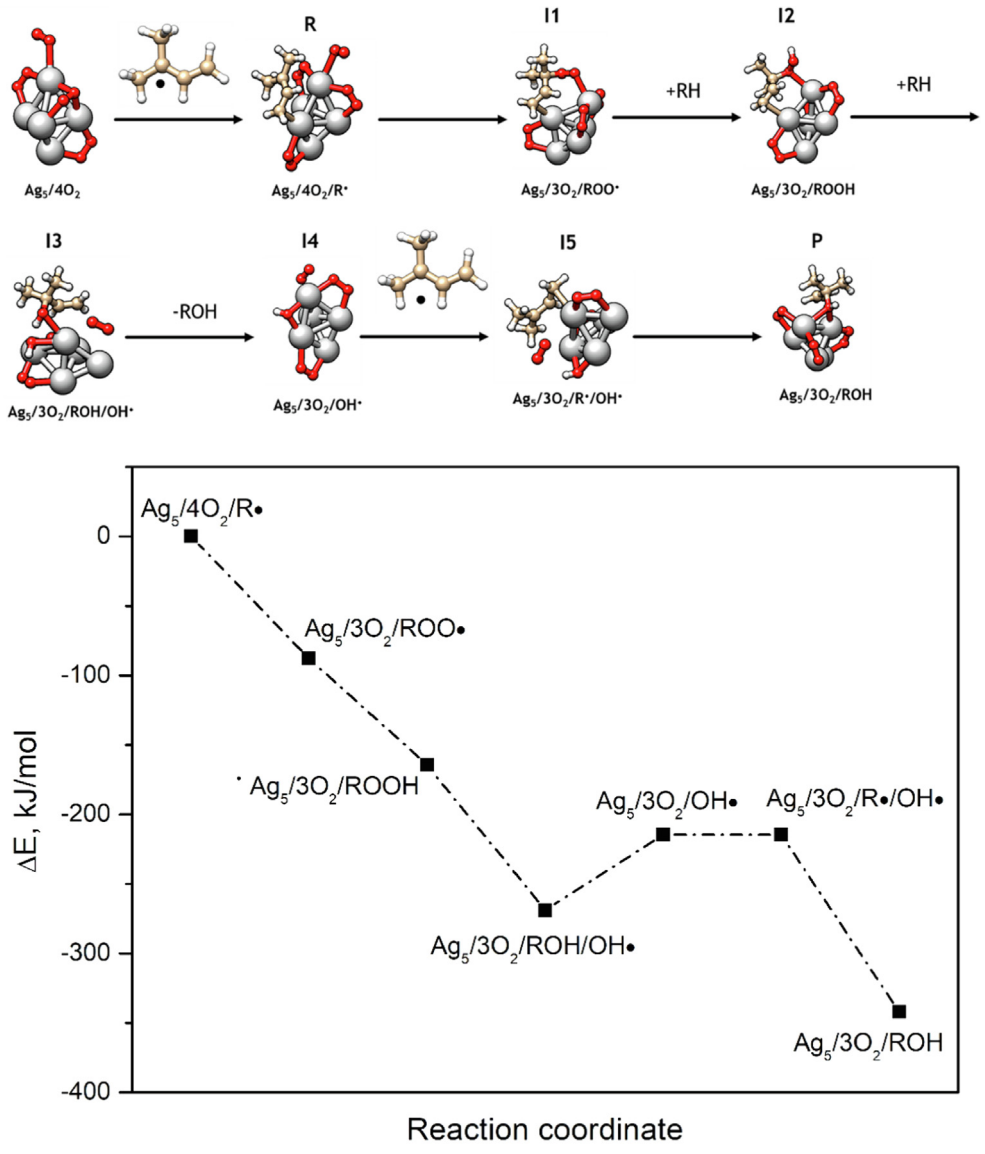

Fig. 7. Top: DFT-optimized structures and bottom: energy balance, for the Ag_5 catalytic PI oxidation process according to scheme plotted on Scheme 1.

attached oxygen molecules is distributed as follows: 1 neutral, 1 superoxo and 2 peroxo/superoxo species. Therefore, we used such more stable species in our theoretical calculations. Proposed reactions and computational results are shown in Fig. 7. The first reaction process is the adsorption of R· on $Ag_5/4O_2$, yielding the $Ag_5/4O_2/R$· system. Once adsorbed, R· reacts with an oxygen molecule placed on an apical position, which is loosely adsorbed on the nanocluster. This process leads to the formation of $Ag_5/3O_2/ROO$· (I1) species with −87 kJ/mol stabilization energy. Spin density analysis revealed that indeed, this molecule is a radical with the unpaired electron mainly placed on the oxygen molecule (Table S2). Then, a hydrogen atom from two RH species in the media can be accepted by the radical, forming $Ag_5/3O_2/ROOH$ (I2) and $Ag_5/3O_2/ROH/OH$· (I3) completing the oxidation of the polymer. The hydrogen transfer to remove the radical specie on I2 intermediate is highly favored (-164 kJ/mol). Spin and charge analysis revealed that the presence of an unpaired electron is negligible, in good agreement with the proposed reaction mechanism. Two electrons remain unpaired in I3 structure, corresponding to the unpaired electron of the nanocluster and the unpaired electron of the hydroxyl group. Nonetheless, due to the bonding between them, they remain combined, thus the spin analysis on Table S3 shows that there is no excess spin density on the entire molecule. The desorption process of the ROH moiety is unfavored by + 54 kJ/mol, due to the remaining hydroxyl radical on the system. Nonetheless, adsorption of another R· species, slightly stabilizes the system. Finally, the new R· reacts with the remaining hydroxyl group yielding another oxidated species. The overall oxidation process, in which two oxidated species are obtained in each catalytic cycle, is highly favored by −342 kJ/mol. As a summary we can say that the presence of nanoclusters does not inhibit the oxidation but favours a decomposition that yields inactive products (route b in Scheme 2), in contrast with the more detrimental ketone formation pathway. In particular, the later leads to chain scissions and the ketones themselves which are more sensitive to further oxidation than alcohols [38]. In ABS, the main site of oxidation are the polybutadiene chains, in which the mechanism of oxidation, and therefore the effect of Ag_5 nanoclusters, is expected to be very similar to that discussed for PI.

4. Conclusions

In conclusion, we have demonstrated the high catalytic efficiency of Ag_5 nanoclusters for the deactivation of DPPH· radicals. The reaction proceeds through the reduction of the radicals with the oxidation of the alcohol -used to dissolve DPPH radical- and the corresponding formation of the aldehyde. Using DFT calculations we could deduce a mechanism for this reaction, which seems to proceed through the formation of a complex between the catalyst, Ag_5, and the two reactive species (DPPH· and CH_3O^-) facilitating the electron transfer between them. The reaction proceeds further in a cascade process with the total deactivation of the intermediate radicals and the formation of the products. The observed catalytic deactivation of the DPPH· radical led us to hypothesize a possible application of nanoclusters for inhibiting undesirable radical oxidations, as those occurring in the radical degradation of polymers. Experiments with thin films of PI and ABS exposed to standard simulated photo-ageing conditions, in the presence of Ag_5, showed that nanoclusters clearly diminished the polymer degradation using only ≈ 15 % coverage. Theoretical calculations show that radicals (R·) are catalytically converted into alcohols due to the easy oxygen adsorption and activation by Ag_5. The catalytic effect towards alcohol formation may be considered as a secondary antioxidation effect, that could pave the way to the development of a new class of secondary antioxidants which convert unstable polymer hydroperoxides to stable oxygen containing groups. Alcohol development blocks the formation of species that can initiate further radical reactions. These results open new possibilities for developing a post process inhibition of polymer degradation, for which now there is no efficient procedure.

As a summary, we have shown that Ag_5 nanoclusters are very stable species which can catalyze the complete reduction (as in DPPH·) or oxidation (as in R· -polymer degradation-) of radicals producing ONLY non-radical species. Therefore, such nanoclusters represent a new kind of catalysts with unique anti-radical properties, which could be of large importance for industrial or biomedical applications. It would be interesting to see if nanoclusters of other metals (Au, Cu, Pt, etc.) can be even more active than Ag, showing higher selectivity against specific types of radicals. We hope that these results will encourage the development of new methods for the synthesis of monodisperse clusters of other metals.

CRediT authorship contribution statement

Iria R. Arias: Visualization, Investigation, Writing – original draft. **David Buceta:** Conceptualization, Methodology, Visualization, Supervision. **Giampaolo Barone:** Methodology, Software. **María C. Giménez-López:** Methodology. **Héctor Lozano:** Methodology, Software, Writing – original draft. **Massimo Lazzari:** Writing – original draft, Methodology, Project administration. **M. Arturo López-Quintela:** Supervision, Writing – review & editing, Project administration.

Data availability

No data was used for the research described in the article.

Declaration of Competing Interest

The authors declare the following financial interests/personal relationships which may be considered as potential competing interests: M. Arturo Lopez-Quintela reports financial support was provided by Government of Galicia Department of Culture Education and Universities. M. Arturo Lopez-Quintela reports financial support was provided by European Union. Massimo Lazzari reports financial support was provided by European Union. David Buceta reports financial support was provided by Government of Galicia Department of Culture Education and Universities. Massimo Lazzari reports financial support was provided by Government of Galicia Department of Culture Education and Universities. Iria Rodriguez reports financial support was provided by Government of Galicia Department of Culture Education and Universities.

Acknowledgements

This research was partially supported by the Consellería de Educación (Xunta de Galicia), Grants No. Grupos Ref. Comp. ED431C 2017/22, ED431C 2019/13 and AEMAT-ED431E2018/08 to M.A.L.Q. The European Union's Horizon 2020 Research and Innovation Programme (Bac-To-Fuel) under Grant Agreement No. 825999 (M.A.L.Q.). The European Union H2020 project Nanorestart (646063), the Xunta de Galicia (Centro singular de investigación de Galicia accreditation 2019-2022, ED431G 2019/03; Consolidación e estructuración ED431B 2018/16) and the European Union (European Regional Development Fund—ERDF) (M.L.). DB expresses gratitude for a postdoctoral grant from Xunta de Galicia, Spain (POS-A/2013/018). I.R.A. express gratitude for a predoctoral grant from Xunta de Galicia.

Appendix A. Supplementary material

Supplementary data to this article can be found online at https://doi.org/10.1016/j.jcis.2022.07.133.

References

[1] Protected Metal Clusters: From Fundamentals to Applications, Tatsuya Tsukuda Hannu Häkkinen, Ed., Elsevier, Amsterdam, 2015.
[2] P. Jena, Q. Sun, Super atomic clusters: design rules and potential for building blocks of materials, Chem. Rev. Am. Chem. Soc. 118 (11) (2018) 5755–5870.
[3] E.C. Tyo, S. Vajda, Catalysis by clusters with precise numbers of atoms, Nat Nano 10 (7) (2015) 577–588.
[4] L. Liu, A. Corma, Metal catalysts for heterogeneous catalysis: from single atoms to nanoclusters and nanoparticles, Chem. Rev. Am. Chem. Soc. 118 (10) (2018) 4981–5079.
[5] Y. Piñeiro, D. Buceta, J. Calvo, S. Huseyinova, M. Cuerva, Á. Pérez, B. Domínguez, M.A. López-quintela, Large stability and high catalytic activities of sub-Nm metal (0) clusters: implications into the nucleation and growth theory, J. Colloid Interface Sci. 449 (2015) 279–285, https://doi.org/10.1016/j.jcis.2015.01.001.
[6] V. Porto, E. Borrajo, D. Buceta, C. Carneiro, S. Huseyinova, B. Domínguez, K.J.E. Borgman, M. Lakadamyali, M.F. Garcia-Parajo, J. Neissa, T. García-Caballero, G. Barone, M.C. Blanco, N. Busto, B. García, J.M. Leal, J. Blanco, J. Rivas, M.A. López-Quintela, F. Domínguez, Silver atomic quantum clusters of three atoms for cancer therapy: targeting chromatin compaction to increase the therapeutic index of chemotherapy, Adv. Mater. 30 (33) (2018) 1801317, https://doi.org/10.1002/adma.201801317.
[7] S. Huseyinova, J. Blanco, F.G. Requejo, J.M. Ramallo-López, M.C. Blanco, D. Buceta, M.A. López-Quintela, Synthesis of highly stable surfactant-free Cu5 clusters in water, J. Phys. Chem. C 120 (29) (2016) 15902–15908, https://doi.org/10.1021/acs.jpcc.5b12227.
[8] V. Porto, D. Buceta, B. Dominguez, C. Carneiro, E. Borrajo, M. Fraile, N. Dávila-Ferreira, I.R. Arias, J.M. Blanco, J.M. Devida, L.J. Giovanetti, F.G. Requejo, J.C. Hernández, J.J. Calvino, M. López-Haro, G. Barone, A.M. James, T. García-Caballero, D.M. González-Castaño, M. Treder, W. Huber, A. Vidal, M.P. Murphy, M.A. López-Quintela, F. Domínguez, Low atomicity silver clusters as highly selective antitumoral agents through irreversible oxidation of thiols, Adv. Funct. Mater. (2022) 2113028.
[9] U. Heiz, F. Vanolli, A. Sanchez, W.-D. Schneider, Size-dependent molecular dissociation on mass-selected, Supported Metal Clusters. 120 (37) (1998) 9668–9671.
[10] D. Buceta, S. Huseyinova, M. Cuerva, H. Lozano, L.J. Giovanetti, J.M. Ramallo-López, P. López-Caballero, A. Zanchet, A.O. Mitrushchenkov, A.W. Hauser, G. Barone, C. Huck-Iriart, C. Escudero, J.C. Hernández-Garrido, J. Calvino, M. Lopez-Haro, M.P. de Lara-Castells, F.G. Requejo, M.A. López-Quintela, Outstanding nobility observed in Cu5 clusters reveals the key role of collective quantum effects, ChemRxiv (2021), https://doi.org/10.26434/CHEMRXIV.13661081.V1.
[11] A. Corma, P. Concepción, M. Boronat, M.J. Sabater, J. Navas, M.J. Yacaman, E. Larios, A. Posadas, M.A. López-Quintela, D. Buceta, E. Mendoza, G. Guilera, A. Mayoral, Exceptional oxidation activity with size-controlled supported gold clusters of low atomicity, Nat. Chem. 5 (September) (2013) 775–781.
[12] J. Lalevée, J.P. Fouassier, Overview of Radical Initiation, Encyclopedia of Radicals in Chemistry, Biology and Materials, January 13, 2012. https://doi.org/https://doi.org/10.1002/9781119953678.rad003.
[13] M. Valko, C.J. Rhodes, J. Moncol, M. Izakovic, M. Mazur, Free radicals, metals and antioxidants in oxidative stress-induced cancer, Chem. Biol. Interact. 160 (1) (2006) 1–40, https://doi.org/10.1016/j.cbi.2005.12.009.
[14] S.P. Hussain, L.J. Hofseth, C.C. Harris, Radical causes of cancer, Nat. Rev. Cancer 3 (4) (2003) 276–285, https://doi.org/10.1038/nrc1046.
[15] B. Halliwell, Role of free radicals in the neurodegenerative diseases, Drugs Aging 18 (9) (2001) 685–716, https://doi.org/10.2165/00002512-200118090-00004.
[16] N.A. Porter, S.E. Caldwell, K.A. Mills, Mechanisms of free radical oxidation of unsaturated lipids, Lipids 30 (4) (1995) 277–290, https://doi.org/10.1007/BF02536034.
[17] G. Scott, Initiation processes in polymer degradation, Polym. Degrad. Stab. 48 (3) (1995) 315–324, https://doi.org/10.1016/0141-3910(95)00090-9.
[18] G. Gryn'ova, J.L. Hodgson, M.L. Coote, Revising the mechanism of polymer autooxidation, Org. Biomol. Chem. 9 (2) (2011) 480–490.
[19] J.C.J. Bart, Additives in Polymers: Industrial Analysis and Applications, John Wiley & Sons, Wiley: Chichester, UK, 2005.
[20] H.G. Schmarr, T. Potouridis, S. Ganß, W. Sang, B. Köpp, U. Bokuz, U. Fischer, Analysis of carbonyl compounds via headspace solid-phase microextraction with on-fiber derivatization and gas chromatographic-ion trap tandem mass spectrometric determination of their O-(2,3,4,5,6-pentafluorobenzyl)oxime derivatives, Anal. Chim. Acta 617 (1–2) (2008) 119–131, https://doi.org/10.1016/J.ACA.2008.02.002.
[21] Y. Zhao, D.G. Truhlar, The M06 suite of density functionals for main group thermochemistry, thermochemical kinetics, noncovalent interactions, excited states, and transition elements: two new functionals and systematic testing of four M06-class functionals and 12 other function, Theor. Chem. Acc. 120 (1–3) (2008) 215–241, https://doi.org/10.1007/s00214-007-0310-x.
[22] M. Kanti Si, A. Sen, B. Ganguly, Exploiting hydrogen bonding interactions to probe smaller linear and cyclic diamines binding to G-quadruplexes: a DFT and molecular dynamics study, Phys. Chem. Chem. Phys. 19 (18) (2017) 11474–11484, https://doi.org/10.1039/C7CP00472A.
[23] F. Weigend, Accurate coulomb-fitting basis sets for H to Rn, Phys. Chem. Chem. Phys. 8 (9) (2006) 1057–1065, https://doi.org/10.1039/B515623H.
[24] M.J. Frisch, G.W. Trucks, H.B. Schlegel, G.E. Scuseria, M.A. Robb, J.R. Cheeseman, G. Scalmani, V. Barone, G.A. Petersson, H. Nakatsuji, X. Li, M. Caricato, A. Marenich, J. Bloino, B.G. Janesko, R. Gomperts, B. Mennucci, H.P. Hratchian, J.V. Ort, W. C. Gaussian 09, Revision E.01, 2016.
[25] J. Tomasi, B. Mennucci, R. Cammi, Quantum mechanical continuum solvation models, Chem. Rev. 105 (8) (2005) 2999–3094, https://doi.org/10.1021/cr9904009.
[26] F.L. Hirshfeld, Bonded-atom fragments for describing molecular charge densities, Theor. Chim. Acta 44 (2) (1977) 129–138, https://doi.org/10.1007/BF00549096.
[27] T. Iwasita, Electrocatalysis of methanol oxidation, Electrochim. Acta 47 (22) (2002) 3663–3674, https://doi.org/10.1016/S0013-4686(02)00336-5.
[28] J.M. Tatibouët, Methanol oxidation as a catalytic surface probe, Appl. Catal. A Gen. 148 (2) (1997) 213–252, https://doi.org/10.1016/S0926-860X(96)00236-0.
[29] G. Mårdh, A.L. Dingley, D.S. Auld, B.L. Vallee, Human class II (Pi) alcohol dehydrogenase has a redox-specific function in norepinephrine metabolism, Proc. Natl. Acad. Sci. U. S. A. 83 (23) (1986) 8908–8912, https://doi.org/10.1073/pnas.83.23.8908.
[30] Q.-T. Nguyen, E. Romero, W.P. Dijkman, S.P. de Vasconcellos, C. Binda, A. Mattevi, M.W. Fraaije, Structure-based engineering of phanerochaete chrysosporium alcohol oxidase for enhanced oxidative power toward glycerol, Biochemistry 57 (43) (2018) 6209–6218, https://doi.org/10.1021/acs.biochem.8b00918.
[31] Y. Chong, C. Ge, G. Fang, X. Tian, X. Ma, T. Wen, W.G. Wamer, C. Chen, Z. Chai, J. J. Yin, Crossover between anti- and pro-oxidant activities of graphene quantum dots in the absence or presence of light, ACS Nano 10 (9) (2016) 8690–8699, https://doi.org/10.1021/ACSNANO.6B04061/SUPPL_FILE/NN6B04061_SI_001.PDF.
[32] V. Sindhi, V. Gupta, K. Sharma, S. Bhatnagar, R. Kumari, N. Dhaka, Potential applications of antioxidants – a review, J. Pharm. Res. 7 (9) (2013) 828–835, https://doi.org/10.1016/J.JOPR.2013.10.001.
[33] N.S. Allen, M. E. Fundamentals of Polymer Degradation and Stabilization, Elsevier, London, 1992.
[34] M. Gómez, D. Reggio, M. Lazzari, Detection of degradation markers from polymer surfaces by a novel SERS-based strategy, Talanta 191 (2019) 156–161, https://doi.org/10.1016/j.talanta.2018.08.046.
[35] L. Gonon, J.-L. Gardette, Photooxidation mechanism of styrene-isoprene copolymer: evolution of the profile of oxidation according to the composition, Polymer (Guildf). 41 (5) (2000) 1669–1678, https://doi.org/10.1016/S0032-3861(99)00346-8.
[36] J.K. Kochi, Oxidation of allylic radicals by electron transfer: effect of complex copper salts, J. Am. Chem. Soc. 84 (17) (1962) 3271–3277, https://doi.org/10.1021/ja00876a012.
[37] M. Lazzari, D. Scalarone, V. Castelvetro, F. Signori, O. Chiantore, Novel partially fluorinated copolymers: evidence of the effect of fluorine on the reactivity of the unfluorinated comonomer units, Macromol. Rapid Commun. 26 (2) (2005) 75–81, https://doi.org/10.1002/marc.200400479.
[38] J.D. Coyle, H.A.J. Carless, Selected aspects of photochemistry. i photochemistry of carbonyl compounds, Chem. Soc. Rev. 1 (4) (1972) 465–480, https://doi.org/10.1039/CS9720100465.